DOI: 10.1002/ejic.200501130

Tetranuclear Complexes Containing a Luminescent Ru_2M_2 Core [M = Cu^I, (allyl)Pd^{II}]: Synthesis, Structures and Electrochemical Properties

Dirk Walther,*[a] Lars Böttcher,[a] Jörg Blumhoff,[a] Sebastian Schebesta,[a] Helmar Görls,[a] Katrin Schmuck,[a] Sven Rau,[a] and Manfred Rudolph[a]

Keywords: Copper / Luminescence / N ligands / Palladium / Ruthenium

The reaction between $[(tbbpy)_2Ru(tmbiH_2)](PF_6)_2$ (tbbpy = 4,4′-di-*tert*-butyl-2,2′-bipyridine; $tmbiH_2$ = 5,5′,6,6′-tetramethyl-2,2′-dibenzimidazole) and LiMe/CuI affords the tetranuclear complex **1** containing the dication $[\{(tbbpy)_2Ru(tmbi)\}_2Cu_2]^{2+}$. The X-ray structure of **1** shows that the two $[(tbbpy)_2Ru(tmbi)]$ units coordinate the two Cu atoms in a twofold monodentate manner. Each copper atom is surrounded by two N-donor atoms of different ruthenium(II) units with N–Cu–N angles of 167.3°. The Cu···Cu separation (2.72 Å) indicates intranuclear contacts. LiMe/$[(allyl)PdCl]_2$ reacts with the starting Ru complex to form **2**, which contains the tetranuclear dication $[\{(tbbpy)_2Ru(tmbi)\}_2\{Pd(\eta^3\text{-allyl})\}_2]^{2+}$. Its crystal structure shows that the Ru^{II} units act as twofold monodentate ligands as well. Each Pd^{II} is in an essentially planar coordination environment containing two nitrogen atoms of two different dibenzimidazolates in the *cis* position with the η^3-bonded allyl group occupying the two remaining positions. In contrast to **1**, where the Ru–Cu–Cu–Ru unit forms an essentially planar structure, a strongly bent structure is formed in compound **2**. ESI mass spectra of **1** and **2** clearly show that the tetranuclear complexes are present in solution as well. Both complexes are luminescent. In addition, **2** catalyses the Heck coupling at 120 °C in *N*,*N*-dimethylacetamide. In contrast to **1** and **2**, the homodinuclear complex $[(tbbpy)_2Ru(tmbi)Ru(tbbpy)_2]$ (**3**) contains the dibenzimidazolate as a twofold chelating ligand that forms two five-membered chelate rings with the Ru centres. Electrochemical measurements of **2** show two reversible, one-electron oxidation steps, the difference between which (ΔE = 89 mV) is distinctly larger than the pure entropic effect. Furthermore, four reduction steps are observed, the first two of which are fully reversible.

Introduction

The construction of oligonuclear metal complexes containing at least two different metals on the opposite side of bridging ligands is an area of general interest not only from synthetic, structural or theoretical points of view but also due to their potential catalytic properties, which often may be different from the related mononuclear species.[1,2] Of special interest in this field is the development of supramolecular combinations consisting of both a photo-redoxactive metal unit (M^1) and a reactive metal (M^2) connected by bridging ligands that allow electronic communication between the metal centers (for a review see ref.[3]). In these complexes the unit M^1 may act as a sensor of reactions at the reactive metal M^2. Furthermore, such systems are interesting candidates for studying directional photoelectron transfer processes between the different metals. In addition, in this type of complex the reactivity of M^2 may not only be tuned by steric or electronic influences of the M^1 units but also by light.[4] An attractive application of this effect would be the development of new photoswitchable catalysts.

We report here on the synthesis, structures and spectroscopic and electrochemical measurements of the two tetranuclear complexes **1** and **2** consisting of two peripheral photoactive $(tbbpy)_2Ru^{II}$ fragments ("M^1"), a tetramethyldibenzimidazolate bridging ligand, and either Cu^I or (allyl)Pd^{II} as reactive metal centres ("M^2"). In these combinations the bridging system is expected to allow electronic communication between the metals on each side.

Results and Discussion

Syntheses and Structures of Complexes 1 and 2

Very recently we have described the new ruthenium complex $[(tbbpy)_2Ru(tmbiH_2)](PF_6)_2$ (tbbpy = 4,4′-di-*tert*-butyl-2,2′-bipyridine; $tmbiH_2$ = 5,5′,6,6′-tetramethyl-2,2′-dibenzimidazole), which is easily accessible by a microwave-assisted reaction.[5] In contrast to the unsubstituted derivative, $[(tbbpy)_2Ru(tmbiH_2)](PF_6)_2$ is more soluble in organic solvents due to the presence of ten methyl groups at the periphery of the complex. Furthermore, the complex contains a free coordination side and should therefore be able

[a] Institut für Anorganische und Analytische Chemie der Friedrich-Schiller-Universität,
Lessingstraße 8, 07743 Jena, Germany
Fax: +49-3641-948-172
E-mail: Dirk.Walther@uni-jena.de

to act as a "metalloligand" after deprotonation, analogous to similar systems (for typical Ru complexes of this type see refs.[5–15]).

The copper(I) complex **1** was obtained as follows. Treatment of $[(tbbpy)_2Ru(tmbiH_2)](PF_6)_2$ in THF with a mixture of copper iodide and methyllithium (molar ratio 1:2) dissolved in diethyl ether at –78 °C resulted in a dark-red solution from which **1** was obtained as a crystalline brown solid after workup. Its electrospray mass spectrum (ESI-MS) performed in $CHCl_3/CH_3OH$ reveals one major peak at *m*/*z* 2123 corresponding to the composition $[\{(tbbpy)_2Ru(tmbi)\}_2Cu_2(PF_6)]^+$, which suggests a structure of the dication according to Figure 1. The calculated isotopic pattern for this tetranuclear species agrees well with the experimentally found one.

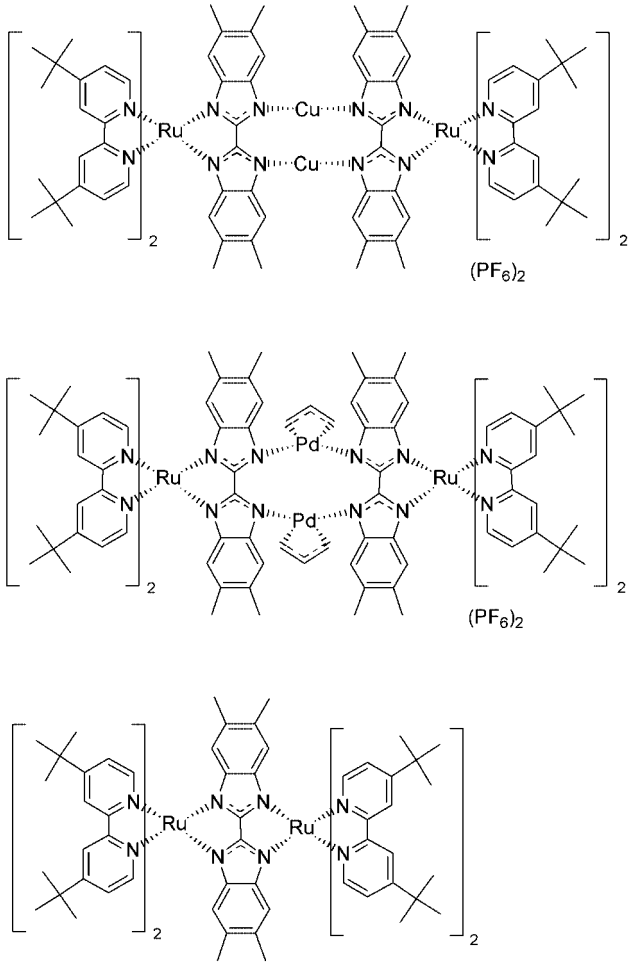

Figure 1. The cations of complexes **1**, **2** and **3**.

The ^1H NMR spectrum of **1** in $CDCl_3$ shows the typical resonances for the $[Ru(tbbpy)_2(tmbi)]$ moiety[5,6] although it gives little additional structural information about **1**. It displays two singlets for the methyl protons of the *tert*-butyl groups at δ = 1.34 and 1.47 ppm, and two singlets for the methyl protons of the bridging ligand at δ = 2.01, and 2.30 ppm in the expected intensity ratio of 3:3:1:1. The protons for the 2,2′-bipyridine system show the expected set of six signals for H3, H3′, H5, H5′, H6, H6′, respectively. Furthermore, two resonances are observed for the aromatic protons of the bridging tmbi at δ = 5.36 and 7.66 ppm. In comparison with the mononuclear complex $[(tbbpy)_2Ru(tmbiH_2)](PF_6)_2$, the corresponding signals in **1** are only slightly low-field shifted.

We succeeded in growing single crystals of the complex **1**, which crystallizes with the anions PF_6^- and Cl^- and with some solvent molecules. Figure 2 shows the solid-state structure of the dication of **1** determined by a low-temperature X-ray analysis and contains relevant bond lengths and angles in the caption.

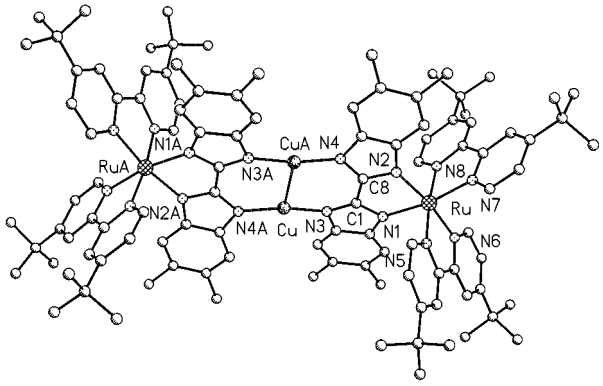

Figure 2. Molecular structure of the dication of complex **1** (the H atoms have been omitted for clarity). Selected bond lengths [Å]: Cu–CuA 2.720(1), Cu–N3 1.852(5), Cu–N4A 1.850(5), Ru–N1 2.087(5), Ru–N2 2.076(5), Ru–N5 2.036(5), Ru–N6 2.041(5), Ru–N7 2.054(6), Ru–N8 2.046(5), C1–C8 1.436(8). Symmetry transformations used to generate equivalent atoms: A $-x+1$, $-y+1$, $-z+1$.

The most remarkable feature is that the two metalloligands do not act as chelating ligands for Cu^I but bind the two Cu atoms in a monodentate manner resulting in an N–Cu–N coordination for each copper(I) centre. There is no additional interaction with the anions. The considerable deviation of the N–Cu–N angles (167.3°) from linearity may be explained by the influence of the other Cu^I centre, which is in close proximity. The Cu···Cu separation is 2.72 Å, which suggests intramolecular contacts (van der Waals radii: 2.8 Å[16]). The Ru···Ru separation is 11.36 Å. Furthermore, the bridging imidazolato rings are essentially planar, and their C–N bond lengths are equal within the experimental error. Since the benzene rings do not lie in this plane, the two tetramethyldibenzimidazolate systems have a boat form with an angle of 163.9° for the centroids of C1–C8, C4–C5 and C11–C12, and C1A–C8A, C4A–C5A and C11A–C12A, respectively.

In addition, the atoms N3–Cu–N4A–N3A–CuA–N4 lie in a plane with extremely small deviations of the Cu atoms from this plane (0.012 Å). The nitrogen atoms N1 and N2, which are coordinated to the $[(tbbpy)_2Ru]$ fragment, lie above this plane (Cu–N3–N1 = 166.6°); the other pair of nitrogen atoms N1A and N2A, which are coordinated to the $[(tbbpy)_2Ru(A)]$ moiety, lies below this plane resulting in a chair arrangement of the eight nitrogen atoms of the two bridging ligands. The unidentate coordination of bridging imidazolates has already been described for a number

of complexes with other metals, although not with Cu^{I}.[1,7] For example, a similar coordination mode for a disilver complex containing π-acidic [2-(phenylazo)pyridine]$_2$Ru fragments at the periphery and the unsubstituted diimidazolate as bridging ligand was recently described by Goswami et al.[7] Furthermore, in a hexametallic Cu^{II} complex containing two Cu^{II} centres and four (bipy)$_2$Ru(bimidazolate) units the diimidazolates also act as monodentate ligands.[8]

Although **1** is coordinatively unsaturated, it does not react with triphenylphosphane. Furthermore, in the solid state no reaction with air was observed.

Treatment of [Ru(tbbpy)$_2$(tmbiH$_2$)](PF$_6$)$_2$ in THF with two equivalents of methyllithium at –78 °C and subsequent treatment with a slight excess of dimeric (allyl)palladium(II) chloride resulted in a dark-red/violet solution from which reddish-brown crystals of **2** were obtained. The ESI mass spectrum performed in $CHCl_3$/CH_3OH showed an envelope of peaks at *m*/*z* 2292 that match well with the isotopic distribution calculated for the fragment ion [{(tbbpy)$_2$-Ru(tmbi-H)}$_2${Pd(allyl)$_2$}(PF$_6$)]$^+$. This indicates that a tetranuclear complex similar to **1** is present in solution as well. The ^{1}H NMR spectrum of **2** in CD_2Cl_2 shows the typical pattern for the [Ru(tbbpy)$_2$(tmbi)] fragments, with the methyl proton signals at δ = 1.37 and 1.53 ppm and the methyl protons of the dibenzimidazolate at δ = 2.03 and 2.33 ppm. In comparison with **1**, these signals and the resonances for the bipy protons and for the aryl signal H7 are shifted slightly downfield.

Single crystals of **2** suitable for an X-ray determination were grown from a mixture of dichloromethane and methanol in the presence of a small amount of water by slow diffusion of dichloroethane into this mixture. Under these conditions, the tetranuclear diaction [{(tbbpy)$_2$Ru-(tmbi-H)}$_2${Pd(allyl)$_2$}]$^{2+}$ crystallizes with both the PF$_6^-$ and the Cl$^-$ anions and with different solvent molecules. Figure 3 shows the molecular structure of the dication and contains relevant bond lengths and angles in the caption.

The two halves of the molecule form an extremely unsymmetrical structure. Similar to complex **1**, the (tbpby)$_2$-Ru(tmbi) metalloligand coordinates in a twofold monodentate manner to the two Pd^{II} centres. Each Pd^{II} is in a distorted planar coordination environment formed by two nitrogen atoms of two different dibenzimidazolates in *cis* positions while the η^3-bonded allyl group occupies the two remaining positions. The two C_2PdN_2 planes are not parallel to each other but are strongly twisted, with a torsion angle of 46.9°. The Pd···Pd separation of 3.06 Å is rather short, suggesting a weak interaction between these metals. The intramolecular Ru···Ru separation is 8.308 Å. In contrast to complex **1**, where the Ru–Cu–Cu–Ru atoms form a planar structure, in compound **2** a strongly bent structure is found. The centroids of the two Pd atoms and the two Ru centres form an angle of 90.7°.

Other bond lengths and angles are in good agreement with typical values found for similar complexes (Figure 3). It is interesting to note that a long-known tetranuclear Pd complex in which four (allyl)Pd^{II} moieties are connected via two dibenzimidazolate bridges has a related structure.[17] In this compound, each of the two imidazolates coordinates an (allyl)Pd^{II} unit to form a chelate ring whereas the other two Pd centres are monodentately coordinated. Although no X-ray studies have been carried out, other mixed complexes containing Pd and Rh may have a similar tetranuclear arrangement.[17] Additionally, related structures have been found in a tetranuclear rhodium carbonyl complex with diimidazolate bridges[18] and in the complex [(η^6-*p*-cumene)ClRu(μ-bbzim)Rh(norbornadiene)$_2$].[1]

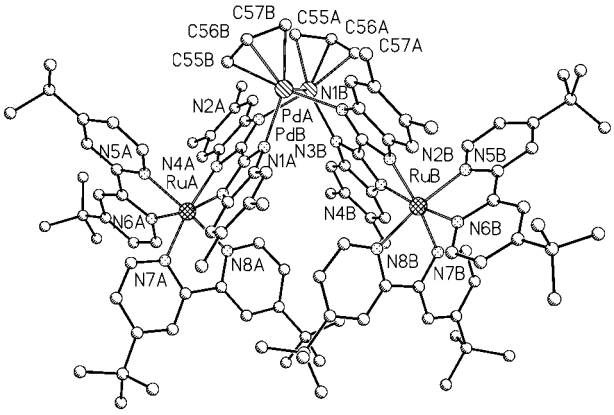

Figure 3. Molecular structure of the dication of complex **2** (the H atoms, the anions PF$_6^-$ and Cl$^-$, and some atom labels have been omitted for clarity). Selected bond lengths [Å]: PdA–N2A 2.092(6), PdA–N3B 2.085(6), PdB–N1A 2.091(5), PdB–N1B 2.111(5), PdA–C55A 2.128(9), PdA–C56A 2.089(9), PdA–C57A 2.096(10), RuA–N4A 2.082(6), RuA–N5A 2.047(6), RuA–N6A 2.049(6), RuA–N7A 2.048(5), RuA–N8A 2.049(6), C1A–C8A 1.450(9), PdB–C55B 2.124(8), PdB–C56B 2.113(12), PdB–C57B 2.153(8), RuB–N4B 2.086(5), RuB–N5B 2.052(5), RuB–N6B 2.045(5), RuB–N7B 2.036(5), RuB–N8B 2.040(5), C1B–C8B 1.460(10).

In contrast to the observed ligand behaviour in these complexes, the structurally similar oxalamidinate ligands act as normal twofold didentate bridging ligands towards Pd^{II} and Cu, forming five-membered chelate rings.[19–22]

The homodinuclear ruthenium tetramethyldibenzimidazolate complex **3** has been prepared using standard procedures.[9] The fully characterised compound was isolated as a mixture of the *rac* and *meso* diastereomers, which exhibit slightly different ^{1}H NMR signals. In contrast to both **1** and **2**, the dibenzimidazolato ligand in **3** acts as a twofold chelating ligand. The X-ray crystal structure of its *meso* form (not depicted; see Experimental Section) shows the two Ru centres on the opposite side of the diimidazolate bridging ligand with bond lengths and angles that are typical for such chelate complexes, althoughr with one exception: the bridging tetramethyldibenzimidazolate ligand is kinked within the central C–C bond.[9]

Electronic Spectra and Catalytic Behaviour of 1–3

The electronic spectra of **1** in THF show an absorption band in the visible region at λ = 519 nm which can be attributed to a ^{3}MLCT transition from Ru^{II} to the bipy ligand. While the starting compound − the deprotonated

metalloligand $[(tbbpy)_2Ru(tmbi)]^-$ is not luminescent, coordination of Cu^I switches on emission resulting in an emission band at λ = 705 nm. The lifetime of the excited state in THF at room temperature (93 ns) (Table 1) is significantly shorter than that in the protonated compound $[(tbbpy)_2Ru(tmbiH_2)]^{2+}$ (lifetime in THF of 363 ns). We have recently observed a similar behaviour with the unsubstituted dibenzimidazolate complex $[(tbbpy)_2Ru(bbim)]$, which acts as a cation-driven molecular switch due to the formation of emitting systems by reacting with metal ions in solution.[6]

Table 1. Optical and electrochemical data of the complexes **1**–**3** at room temperature.

	Complex **1**	Complex **2**	Complex **3**
Absorption λ_{max} [nm][a]	519	524	515
Emission λ_{max} [nm][b]	705	653	707
Lifetime [ns][c]	93[d]	244[d]	60[e]
$E^{[f]}_{1/2}$ (ox) [V]	dec.	+0.146, +0.235	+0.215, +0.51
$E^{[f]}_{1/2}$ (red) [V]	dec.	–1.989, –2.036	–1.963, –2.027
		–2.313, –2.385	–2.260, –2.338

[a] ±2 nm in THF. [b] ±4 nm in THF. [c] ±10%. [d] In THF. [e] In acetonitrile. [f] ±0.004 V in acetonitrile.

In the electronic spectrum of **2** in THF (Table 1) the lowest absorption maximum appears at λ = 524 nm which is only slightly shifted compared with **1**. In contrast, a larger difference was observed in the emission spectra in THF, where the emission maximum was found at λ_{em} = 653 nm, which represents a hypsochromic shift of 52 nm. In addition, the lifetime of the excited state of 244 ns is significantly longer than that for **1**. A more detailed study of the interesting photophysical behaviour of complex **2** will be described in detail in a separate publication.[23]

The homodinuclear complex **3** has the lowest absorption maximum in THF at λ = 515 nm and emits at 707 nm, which compares well with the unsubstituted derivatives.[9]

Preliminary investigations of the catalytic behaviour of **1** and **2** show only low activity of **1** in the catalytic oxidation of 3,5-di-*tert*-butylcatechol to form the *o*-quinone. Complex **2** catalyses the Heck reaction of aryl bromides with substituted aryl olefins. An investigation of the reaction between 4-bromoacetophenone and *n*-butyl acrylate, which is usually chosen as a standard reaction to evaluate the catalyst productivity, at 120 °C in (*N*,*N*-dimethylacetamide) with sodium acetate as the base resulted in 86% conversion after two hours (turnover number: 4300 mol conversion per mol catalyst). At 80 °C the catalysis proceeded slowly, with 37% conversion after 11 h (TON = 1850). In the microwave-assisted Heck coupling 83% conversion was observed after 1 h (TON = 4150; programme 10 s at 175 W, then 1 h at 65 W).

Electrochemistry of Complexes 2 and 3

Due to the decomposition of **1** during the electrochemical measurements the electrochemistry of this complex could not be studied. In contrast, the palladium complex **2** is stable under these conditions and could be investigated electrochemically (Table 1). For comparison, the dimeric ruthenium complex $[(tbbpy)_2Ru(\mu\text{-}tmbi)Ru(tbbpy)_2]$ (**3**) was also investigated. Complex **3** exhibits two chemically reversible one-electron oxidation steps. The half-wave potentials were found to be at +0.215 and +0.51 V with respect to the ferrocene/ferrocenium couple and the diffusion coefficient of the complex, $D_{LRu–RuL}$, amounts to about 5×10^{-6} cm^2 s^{-1}. Formally the two one-electron steps may be attributed to the oxidation of both the ruthenium(II) centres in the complex. The relatively large difference of these potentials (ΔE = 295 mV) shows that there is a remarkable electronic communication between the Ru centres.

At first glance the reduction of complex **3** ("LRu–RuL") shown in Figure 4 seems also to proceed in two separate reduction steps at about –2 and –2.3 V, respectively. However, a more detailed analysis of the frequency dependence of the peak heights and peak shapes (using the diffusion coefficient estimated from the oxidation process) revealed that each peak is actually formed by two overlapping one-electron steps. A comparison of experimental square-wave voltammograms (solid line) and those simulated on the basis of the mechanism (M1; open circles) is shown in Figure 4.

$$\begin{aligned}
&LRu-RuL + e^- \rightleftharpoons LRu-RuL^- \quad (E_1^0 = -1.963\ V)\\
&LRu-RuL^- + e^- \rightleftharpoons L^-Ru-RuL^- \quad (E_2^0 = -2.027\ V)\\
&L^-Ru-RuL^- + e^- \rightleftharpoons L^-Ru-RuL^{2-} \quad (E_3^0 = -2.260\ V)\\
&L^-Ru-RuL^{2-} + e^- \rightleftharpoons L^{2-}Ru-RuL^{2-} \quad (E_4^0 = -2.338\ V)
\end{aligned} \tag{M1}$$

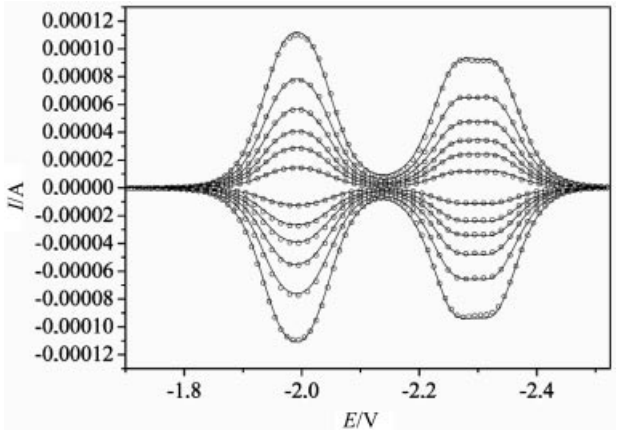

Figure 4. Comparison of experimental (solid line) and simulated (open circles) cyclic square-wave voltammograms for the reduction of a 1.1 mM solution of complex **3** at a mercury drop electrode in acetonitrile. The voltammograms refer to square-wave frequencies of 50, 200, 400, 800, 1500 and 3000 Hz (with increasing peak height) and the potential scale is referenced to the ferrocene/ferrocenium couple. The simulations were executed on the basis of the mechanism M1 with LRu–RuL = complex **3**.

The one-electron steps can be attributed here to the stepwise reduction of the two $(tbbpy)_2Ru$ units involved in the complex assuming fully reversible charge-transfer reactions and identical diffusion coefficients for all species. The dif-

ference $|E_2^0–E_1^0|$ = 64 mV and $|E_4^0–E_3^0|$ = 78 mV is distinctly greater than the limiting value of 35.6 mV resulting from a pure entropic effect. A communication of the complex centres through the bridging ligand is therefore clearly visible in the cathodic charge-transfer processes. Of course, the electronic coupling is even larger if both reduction steps refer to the same $(tbbpy)_2Ru$ moiety ($|E_3^0–E_1^0|$ = 297 mV and $|E_4^0–E_2^0|$ = 311 mV, respectively).

The oxidation of complex **2** by cyclic square-wave voltammetry is shown in Figure 5. This figure reveals that the oxidation of the complex is similar to that reported above for **3**, but in contrast to the latter compound both one-electron steps are no longer well separated. For this reason, reliable results can be evaluated only by subjecting the experimental data to a fitting procedure. The values of the half-wave potentials retrieved for the best fit are +0.146 and +0.235 V, respectively, which is a difference of 89 mV. This value is smaller than that reported above for complex **3** but still distinctly larger than that expected for a pure entropic effect.

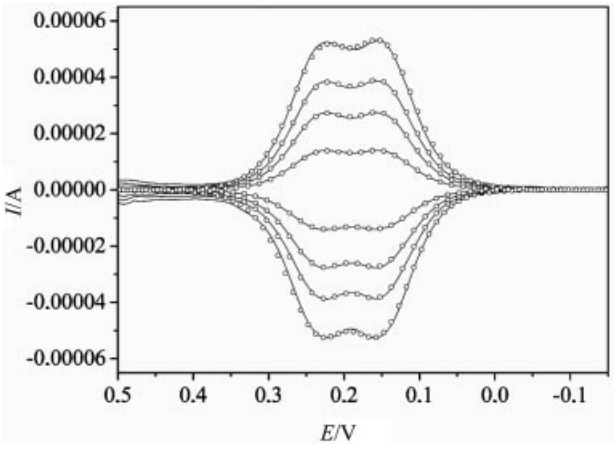

Figure 5. Comparison of experimental (solid line) and simulated (open circles) cyclic square-wave voltammograms for the oxidation of a 1.9 mM solution of complex **2** at a platinum disc electrode in acetonitrile. The voltammograms refer to square-wave frequencies of 50, 200, 400 and 800 Hz (with increasing peak height) and the potential scale is referenced to the ferrocene/ferrocenium couple. The simulations were executed for a reversible E–E mechanism using the standard potentials reported in the text.

The close relationship to the electrochemistry of the LRu–RuL complex **3** also becomes visible when looking at the reduction of **2** using the cyclic square-wave voltammograms (depicted in Figure 6) or at the experiment referring to the highest square-wave frequency ($f_{sw} \geq 200$ Hz) in Figure 7. Figure 6 reveals that the first two one-electron steps proceed in a fully reversible way analogously to that indicated by the first two reactions in (M1) when replacing LRu–RuL by LRu-^{Pd}-RuL as a symbol for complex **2**. The half-wave potentials of these processes (evaluated from the data fitting shown in Figure 6) were estimated to be at $E_1°$ = –1.989 and $E_2°$ = –2.036 V, respectively, which means that $|E_2^0–E_1^0|$ is 47 mV. That means that the deviation from the ideal peak shape of an uncoupled system is hardly visible and is only detectable by fitting current curves referring to different time windows.

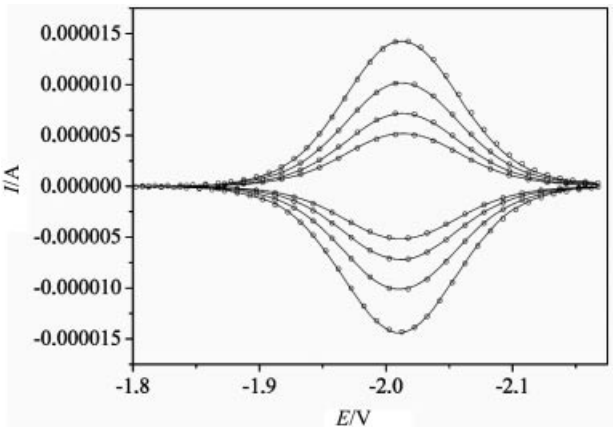

Figure 6. Comparison of experimental (solid line) and simulated (open circles) cyclic square-wave voltammograms for the reduction of a 0.6 mM solution of complex **2** at a mercury-drop electrode in acetonitrile. The voltammograms refer to square wave frequencies of 25, 50, 100 and 200 Hz (with increasing peak height) and the potential scale is referenced with respect to the ferrocene/ferrocenium couple. The simulations were executed taking the first two reactions of the mechanism shown in M2 into consideration.

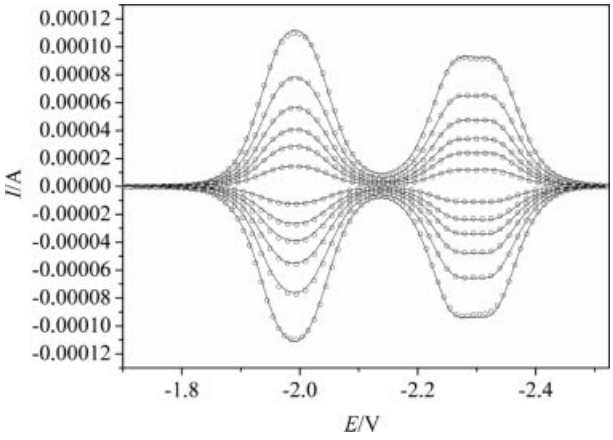

Figure 7. Comparison of experimental (solid line) and simulated (open circles) cyclic square-wave voltammograms for the reduction of a 0.6 mM solution of **2** at a mercury drop electrode in acetonitrile. The voltammograms refer to square wave frequencies of 25, 50, 100 and 200 Hz (with increasing peak height) and the potential scale is referenced with respect to the ferrocene/ferrocenium couple. The simulations were executed taking the reactions M2, M3 and M4 into consideration.

The most striking difference in the electrochemistry of the LRu-^{Pd}-RuL complex **2** compared to that of the LRu–RuL complex **3** becomes visible when looking at the low-frequency experiments shown in Figure 7. While the current response of the high-frequency experiment (f_{sw} = 200 Hz) is, at least qualitatively, very similar to the voltammograms of the LRu–RuL complex depicted in Figure 4, an additional shoulder is more and more noticeable at around –2.05 V upon decreasing the square-wave frequency (i.e. more time is needed before the re-oxidation process to the

starting product takes place). Integrating the cathodic and anodic current in these curves reveals that virtually no charge is lost in the course of the re-oxidation processes. Combining this result with the fact that the first two one-electron steps appear (chemically and electrochemically) fully reversible in Figure 6 gives rise to the conclusion that (after receiving three or four electrons) complex **2** slowly decomposes to another product which is reoxidized and gives the additional shoulder at about –2.05 V. Interestingly, the latter value is very close to one of the reversible half-wave potentials of the deprotonated complex [(tbbpy)$_2$-Ru(tmbi)].[9] This complex exhibits two chemically reversible one-electron reduction steps at –2.07 and –2.364 V, respectively. It therefore appears reasonable to assume that the additional shoulder results from the re-oxidation of reduced [(tbbpy)$_2$Ru(tmbi)] species formed by decomposition of the three- or fourfold reduced complex **3**. Indeed, the experimental square-wave voltammograms shown in Figure 7 (solid lines) are in very good agreement with the simulated ones (open circles) obtained on the basis of a reaction scheme similar to M1

$$\begin{aligned}
&LRu-\overset{Pd}{\underset{Pd}{}}-RuL+e^- \rightleftharpoons LRu-\overset{Pd}{\underset{Pd}{}}-RuL^- \quad (E_1^0 = -1.989\ V)\\
&LRu-\overset{Pd}{\underset{Pd}{}}-RuL^- + e^- \rightleftharpoons L^-Ru-\overset{Pd}{\underset{Pd}{}}-RuL^- \quad (E_2^0 = -2.036\ V)\\
&L^-Ru-\overset{Pd}{\underset{Pd}{}}-RuL^- + e^- \rightleftharpoons L^-Ru-\overset{Pd}{\underset{Pd}{}}-RuL^{2-} \quad (E_3^0 = -2.313\ V)\\
&L^-Ru-\overset{Pd}{\underset{Pd}{}}-RuL^{2-} + e^- \rightleftharpoons L^{2-}Ru-\overset{Pd}{\underset{Pd}{}}-RuL^{2-} \quad (E_4^0 = -2.385\ V)
\end{aligned} \qquad (M2)$$

but includes the decomposition reaction. (Actually, it cannot really be distinguished from the experimental data whether the decomposition reaction starts with the third or only after the fourth reduction step. For convenience, only one follow-up reaction has been taken into consideration.)

$$L^{2-}Ru-\overset{Pd}{\underset{Pd}{}}-RuL^{2-} \rightarrow RuL^{2-} + RuL^{2-} \qquad (M3)$$
$$(k \approx 1\ s^{-1})$$

In the backward scan the re-oxidation proceeds simultaneously by two pathways: firstly, as indicated in M2, and secondly, as re-oxidation of the decomposition products.

$$\begin{aligned}
&RuL^- + e^- \rightleftharpoons RuL^{2-} \quad (E_{2'}^0 = -2.358\ V)\\
&RuL + e^- \rightleftharpoons RuL^- \quad (E_{1'}^0 = -2.075\ V)
\end{aligned} \qquad (M4)$$

The fact that the half-wave potentials $E_{1'}^0$ and $E_{2'}^0$ retrieved by the fitting routine are, within the experimental error, in agreement with those reported above for the deprotonated complex [(tbbpy)$_2$Ru(tmbi)] is a strong indication that the latter species is really formed by the follow-up reaction (M3).

Conclusions

The tetranuclear complexes **1** and **2** are built up by connecting two (tbbpy)$_2$Ru^{II}(tetramethyldiimidazolate) fragments by either Cu^{I} centres or two (allyl)Pd^{II} fragments. In these complexes the dibenzimidazolates act as twofold monodentate ligands resulting in 10-membered metallamacrocycles, which are luminescent at room temperature. Electrochemical measurements show that there is an electronic communication between the Ru centres in **2**. Complex **2** is a good catalyst for the Heck reaction in the dark.

Experimental Section

General Procedures: Infrared spectra were recorded with a Perkin–Elmer 2000 FT-IR, ^{1}H NMR spectra were recorded with a Bruker 400 MHz/200 MHz spectrophotometer and UV/Vis spectra were obtained with a Varian Cary 1 UV/Vis or Shimadzu UV 3100 UV/Vis-NIR. The mass spectra were recorded with a SSQ 170, Finnigan Mat spectrometer. Electrospray mass spectra were recorded with a Finnnigan MAT, MAT 95 XL. Values quoted for *m*/*z* are for the most intense peak of the isotope envelope. The measured isotopic pattern for complexes **1** and **2** are in good agreement with the isotopic pattern calculated using the program ICIS (version 8.2.1, Finnigan). Emission spectra were recorded with a Perkin–Elmer LS50B spectrometer equipped with a Hamamatsu R928 red-sensitive detector.

All manipulations were carried out by using modified Schlenk techniques under an atmosphere of argon. Prior to use, THF, diethyl ether and *n*-pentane were dried with potassium hydroxide and distilled from over sodium/benzophenone. Methyllithium (1.6 M solution in diethyl ether, Fluka), 4-bromoacetophenone (Fluka) and sodium acetate (Aldrich) were used as received; [(tbbpy)$_2$Ru-(tbbpy)$_2$Cl$_2$] and [(tbbpy)$_2$Ru(tmbiH$_2$)](PF$_6$)$_2$ was prepared according to a literature procedure.[5]

Complex 1: A stirred suspension of bis(4,4′-di-*tert*-butyl-2,2′-bipyridine)-5,6,5′,6′-tetramethyl-2,2′-dibenzimidazolatoruthenium(II) hexafluorophosphate (298 mg, 0.24 mmol) in 30 mL of THF at –78 °C was treated dropwise with a an equimolar amount of lithium dimethylcuprate, prepared by reaction of CuI with MeLi in diethyl ether. The reaction mixture was than stirred for 36 h at room temperature. After filtration the solvent was evaporated and the remaining substance was dried in vacuo. Yield: 266 mg (96%). ^{1}H NMR (CDCl$_3$, 200 MHz): δ = 1.34, 1.47 (s, each 36 H, *tert*-butyl), 2.01, 2.30 (s, each 12 H, CH$_3$ of benzimidazolate), 5.36 (s, 4 H, Ar-H4), 7.15 (dd, ^3J = 6.2, ^4J = 1.8 Hz, 4 H, bipy-H5′), 7.40 (dd, ^3J = 6.2, ^4J = 2.0 Hz, 4 H, bipy-H5), 7.66 (s, 4 H, aryl-H7), 7.75 (d, ^3J = 6.0 Hz, 4 H, bipy-H6′), 7.91 (d, ^3J = 6.2 Hz, 4 H, bipy-H6), 8.13 (d, ^4J = 1.4 Hz, 4 H, bipy-H3′), 8.20 (d, ^4J = 1.8 Hz, 4 H, bipy-H3) ppm. MS (Micro-ESI in CH$_2$Cl$_2$/methanol): *m*/*z* 2123 [M – PF$_6$]$^+$, 990 [M/2 + H – 2PF$_6$]$^+$. Absorption (THF): λ_{max} = 519 nm (intensity = 19526 L mol^{-1} cm^{-1}). Emission (THF): λ_{em} = 705 nm (λ_{ex} = 520 nm); lifetime of the first excited state: 93 ns in THF at room temperature.

Recrystallization from THF/CH$_2$Cl$_2$ resulted in a complex of the composition **1**·2THF·CH$_2$Cl$_2$. C$_{117}$H$_{146}$Cl$_2$CuF$_{12}$N$_{16}$O$_2$Pd$_2$P$_2$Ru$_2$ (2498.4): calcd. C 56.24, H 5.89, N 8.97; found C 55.91, H 5.98, N 8.64. Single crystals of the composition [{(tbbpy)$_2$Ru(tmbi)}$_2$-Cu$_2$](PF$_6$)$_{1.5}$Cl$_{0.5}$·CH$_2$Cl$_2$·2 CH$_3$OH·H$_2$O, were grown from a solution in dichloromethane and methanol in the presence of a small amount of water.

Complex 2: A stirred suspension of bis(4,4′-di-*tert*-butyl-2,2′-bipyridine)-5,6,5′,6′-tetramethyl-2,2′-dibenzimidazolatoruthenium(II) hexafluorophosphate (500 mg, 0.41 mmol) in about 20 mL of THF

was treated dropwise with 0.4 mL of a solution of methyllithium in diethyl ether (1.6 M). Then, (allyl)palladium(II) chloride dimer (100 mg, 0.27 mmol) dissolved in 10 mL of THF was added dropwise at –78 °C. Stirring for about 20 h and evaporation of most the solvent at 0 °C in vacuo gave a dark red precipitate which was dissolved in dichloromethane. After subsequent filtration to remove the lithium salt and evaporation of most of the solvent, complex **2** crystallized as a red, microcrystalline compound. Yield: 432 mg (70%). MS (Micro-ESI in $CHCl_3$/methanol): *m/z* 2292 $[M + H - PF6]^+$, 1073 $[M/2 - 2PF_6]^+$. Absorption (THF): λ_{max} = 524 nm (intensity = 13431 $L\,mol^{-1}\,cm^{-1}$). Emission (THF): λ_{em} = 653 nm (λ_{ex} = 524 nm); lifetime of the first excited state: 244 ns in THF at room temperature. ^1H NMR (CD_2Cl_2, 200 MHz): δ = 1.37, 1,53 (each s, *tert*-butyl), 2.03, 2.33 (each s, CH_3 of benzimidazolate), 3.10, 3.70, 4.20 (broad, m, allyl), 5.41 (s, aryl-H4), 7.40 (m, Ar-H), 7.5–7.6 (m, bipy-5 + aryl-H7), 7.84, 7.87 (each s, bipy-H6, bipy-H6′), 8.22, 8.29 (each d, bipy-H3 and bipy-H3′) ppm. Recrystallization from CH_2Cl_2 resulted in a complex with the composition **2**·4CH_2Cl_2. $C_{118}H_{146}Cl_8F_{12}N_{16}P_2Pd_2Ru_2$ (2776.4): calcd. C 51.03, H 5,30, N 8.07; found C 51.29, H 5.59, N 7.75. Single crystals were grown from a mixture of dichloromethane and methanol in the presence of a small amount of water by slow diffusion of dichloroethane into this mixture.

Complex 3: Complex 3 was obtained by employing the method described for homologous dinuclear dibenzimidazole complexes[9] using $[Ru(tbbpy)_2Cl_2]$ (233 mg, 0.33 mmol) and $tmbiH_2$ (50 mg, 0.165 mmol). After obtaining the pure fractions recrystallization from acetone/water (50:50) yielded the pure complex. Crystals suitable for X-ray diffraction were grown from acetone/water at –20 °C. Under these conditions the *meso* isomer crystallized. Absorption maximum (CH_3CN) at λ_{max} = 512 nm, emission maximum (CH_3CN) at λ_{em} = 709 nm. ^1H NMR (200 MHz, $CDCl_3$): δ = 8.23 (d, *J* = 4.9 Hz, 6 H), 8.16 (m, 8 H), 7.84–7.80 (m, 4 H), 7.72 (d, *J* = 6.8 Hz, 2 H), 7.44–7.37 (m, 6 H), 7.10 (s, 2 H), 2.15 (s, 12 H), 1.45 (s, 36 H), 1.31 (s, 36 H) ppm. MS (ESI in MeOH) *m/z* 781 [M/2 – $2PF_6$] 1562 $[M - 2PF_6]^+$; 1707 $[M - PF_6)]^+$ with the expected isotopic pattern. [**3**(acetone)$_4$(H_2O)$_2$]. $C_{102}H_{140}F_{12}N_{12}O_6P_2Ru_2$ (2122.2): calcd. C 57.77, H 6.65, N 7.92; found C 57.85, H 6.42, N 7.74. Single crystals of the composition [{$(tbbpy)_2Ru(tmbi)_2$}-$(PF_6)_2$] were grown from acetonitrile at –20 °C.

Crystal Structure Determination: The intensity data for the compounds were collected on a Nonius KappaCCD diffractometer using graphite-monochromated Mo-K_α radiation. Data were corrected for Lorentz-polarization effects and for absorption effects.[24–26] The structures were solved by direct methods (SHELXS[27]) and refined by full-matrix least-squares techniques against F_o^2 (SHELXL-97[28]). The hydrogen atoms were included at calculated positions with fixed thermal parameters. All non-hydrogen atoms were refined anisotropically.[28] XP (SIEMENS Analytical X-ray Instruments, Inc.) was used for structure representations.

Crystal Data for 1:[29] $C_{108}H_{128}N_{16}Cu_2Ru_2{\cdot}1.5PF_6{\cdot}0.5Cl{\cdot}4CH_2Cl_2{\cdot}2CH_3OH{\cdot}H_2O$, M_r = 2635.46 $g\,mol^{-1}$, red-brown prism, size 0.04 × 0.04 × 0.04 mm^3, triclinic, space group $P\bar{1}$, *a* = 12.5919(3), *b* = 13.9697(4), *c* = 19.6388(5) Å, *α* = 100.022(2)°, *β* = 93.575(1)°, *γ* = 94.941(1)°, *V* = 3378.7(2) $Å^3$, *T* = –90 °C, *Z* = 1, $\rho_{calcd.}$ = 1.295 $g\,cm^{-3}$, μ(Mo-K_α) = 7.78 cm^{-1}, multi-scan, $transm._{min.}$ = 0.7326, $transm._{max.}$ = 0.8678, *F*(000) = 1359, 21202 reflections in *h*(–16/16), *k*(–18/17), *l*(–25/24), measured in the range 7.13° ≤ *Θ* ≤ 27.46°, completeness Θ_{max} = 91.9%, 14231 independent reflections, R_{int} = 0.040, 10166 reflections with $F_o > 4\sigma(F_o)$, 734 parameters, 0 restraints, R_{1obs} = 0.089, wR_{2obs} = 0.218, R_{1all} = 0.130, wR_{2all} = 0.256, GOOF = 1.027, largest difference peak and hole: 3.510/–1.553 e $Å^{-3}$.

Crystal Data for 2:[29] $C_{114}H_{138}N_{16}Pd_2Ru_2{\cdot}1.5PF_6{\cdot}0.5Cl{\cdot}1.5C_2H_4Cl_2{\cdot}CH_3OH{\cdot}8H_2O$, M_r = 2707.12 $g\,mol^{-1}$, red-brown prism, size 0.06 × 0.06 × 0.05 mm^3, triclinic, space group $P\bar{1}$, *a* = 16.0071(2), *b* = 18.3010(2), *c* = 29.0031(4) Å, *α* = 107.518(1)°, *β* = 95.968(1)°, *γ* = 93.112(1)°, *V* = 8025.5(2) $Å^3$, *T* = –90°C, *Z* = 2, $\rho_{calcd.}$ = 1.120 $g\,cm^{-3}$, μ(Mo-K_α) = 5.36 cm^{-1}, multi-scan, $transm._{min.}$ = 0.8426, $transm._{max.}$ = 0.9778, *F*(000) = 2798, 42423 reflections in *h*(–20/19), *k*(–23/21), *l*(–28/37), measured in the range 2.51° ≤ *Θ* ≤ 27.49°, completeness Θ_{max} = 86.3%, 31794 independent reflections, R_{int} = 0.026, 23991 reflections with $F_o > 4\sigma(F_o)$, 1498 parameters, 0 restraints, R_{1obs} = 0.087, wR_{2obs} = 0.258, R_{1all} = 0.114, wR_{2all} = 0.290, GOOF = 1.027, largest difference peak and hole: 2.862/–1.560 e $Å^{-3}$.

Crystal Data for 3:[29] $C_{90}H_{112}F_{12}N_{12}P_2Ru_2{\cdot}3C_2H_3N$, M_r = 1977.16 $g\,mol^{-1}$, red-brown prism, size 0.04 × 0.04 × 0.03 mm^3, triclinic, space group $P\bar{1}$, *a* = 15.6447(5), *b* = 17.4399(4), *c* = 19.9816(5) Å, *α* = 74.301(2)°, *β* = 80.793(2)°, *γ* = 67.123(2)°, *V* = 4826.4(2) $Å^3$, *T* = –90°C, *Z* = 2, $\rho_{calcd.}$ = 1.361 $g\,cm^{-3}$, μ (Mo-K_α) = 4.22 cm^{-1}, *F*(000) = 2056, 33338 reflections in *h*(–20/19), *k*(–22/21), *l*(–25/24), measured in the range 2.48° ≤ *Θ* ≤ 27.51°, completeness Θ_{max} = 98.6%, 21886 independent reflections, R_{int} = 0.042, 14398 reflections with $F_o > 4\sigma(F_o)$, 1150 parameters, 0 restraints, R_{1obs} = 0.060, wR_{2obs} = 0.128, R_{1all} = 0.109, wR_{2all} = 0.153, GOOF = 1.027, largest difference peak and hole: 0.811/–0.620 e $Å^{-3}$.

Heck Reactions: In a typical experiment, 6.25 mmol of 4-bromoacetophenone and 7 mmol of anhydrous sodium acetate as base were placed in a 25-mL two-necked flask equipped with a stirring bar, reflux condenser and septum. The flask was degassed under vacuum and purged with argon to ensure an inert reaction atmosphere. Then, 10 mL of *N*,*N*-dimethylacetamide as solvent, 0.5 g of diethylene glycol/dibutyl ether as GC standard and 6.75 mmol of *n*-butyl acrylate were added through the septum. The reaction mixture was thoroughly stirred and heated to the appropriate reaction temperature at which it was held for 5 min followed by treatment with the catalyst solution containing complex **2** (1.25 μmol in 0.5 mL of THF). After the appropriate time interval the reaction mixture was hydrolyzed with 2 mL of distilled water and extracted with 2 mL of CH_2Cl_2. The organic phase was dried with K_2CO_3 and stored at –25 °C until GC analysis for determination of the yield. The microwave-assisted Heck coupling was carried out using a Microwave Laboratory Systems MLS EM-2 microwave system (microwave set-up: 10 s at 175 W then 1 h at 65 W).

Electrochemical Measurements: Square-wave voltammetric measurements were conducted using a three-electrode technique with a home-built computer-controlled instrument based on the PCI-6110E data acquisition board (National Instruments). The experiments were performed in acetonitrile containing 0.25 M tetrabutylammonium perchlorate under a blanket of solvent-saturated argon. The ohmic resistance, which had to be compensated for, was determined by measuring the impedance of the system at potentials where the faradaic current was negligibly small. The internal reference electrode was an Ag/AgCl electrode in acetonitrile containing 0.25 M tetrabutylammonium chloride. However, for convenience all potentials are reported with respect to the ferrocene/ferrocenium couple. The working electrode was either a hanging mercury drop ($m_{Hg-drop}$ = 3.8–4.4 mg) produced by the CGME instrument or a 1.5 mm platinum disk electrode (both from Bioanalytical Systems, Inc.,West Lafayette, USA; experimental errors for *E* = ±0.004 V; and for $\Delta E_{1/2}$ = ±0.001 V). The electrochemical experiments were

evaluated by fitting theoretical current curves to experimental ones using the freely available DigiElch software (DigiElch can be freely downloaded from www.DigiElch.de). The theoretical background of the simulation method used in this program has been given in a series of accompanying papers.[30] We assumed in all simulations that the diffusion coefficients of the complexes do not depend on the charge of the complex.

Acknowledgments

Financial support from the Deutsche Forschungsgemeinschaft (SFB, 436) is gratefully acknowledged.

[1] D. Carmona, J. Ferrer, A. Mendoza, F. J. Lahoz, L. A. Oro, *Organometallics* **1995**, *14*, 2066.
[2] M. P. Garcia, A. M. Lopez, M. A. Esteruelas, F. J. Lahoz, L. A. Oro, *Organometallics* **1991**, *10*, 127.
[3] V. Balzani, A. Credi, M. Venturi, *Molecular Devices and Machines*, Wiley-VCH, Weinheim, **2003**.
[4] M. Saito, Y. Nishibayashi, S. Uemura, *Organometallics* **2004**, *23*, 4012.
[5] S. Rau, B. Schäfer, A. Grüßing, S. Schebesta, K. Lamm, J. Vieth, H. Görls, D. Walther, M. Rudolph, U. W. Grummt, E. Birkner, *Inorg. Chim. Acta* **2004**, *357*, 4496.
[6] S. Rau, T. Büttner, C. Temme, M. Ruben, H. Görls, D. Walther, M. Duati, S. Fanni, G. Vos, *Inorg. Chem.* **2000**, *39*, 1621.
[7] P. Majumdar, K. K. Kamar, S. Goswami, A. Castineiras, *Chem. Commun.* **2001**, 1292–1293.
[8] K. K. Kamar, L. R. Falvello, P. E. Fanwick, J. Kim, S. Goswami, *Dalton Trans.* **2004**, 1827.
[9] S. Rau, M. Ruben, T. Büttner, C. Temme, S. Dautz, H. Görls, M. Rudolph, D. Walther, A. Brotkorb, M. Duati, C. O'Connor, J. G. Vos, *J. Chem. Soc., Dalton Trans.* **2000**, 3649.
[10] S. Rau, B. Schäfer, S. Schebesta, A. Grüßing, W. Poppitz, D. Walther, M. Duati, W. R. Browne, J. G. Voss, *Eur. J. Inorg. Chem.* **2003**, 1503.
[11] M. Haga, *Inorg. Chim. Acta* **1980**, *45*, L183.
[12] M. Haga, *Inorg. Chim. Acta* **1983**, *75*, 29.
[13] A. M. Bond, M. Haga, *Inorg. Chem.* **1986**, *25*, 4507.
[14] M. Haga, T. Matsamura-Inoue, S. Yamabe, *Inorg. Chem.* **1987**, *26*, 4148.
[15] D. P. Rillema, R. Sahai, P. Matthews, A. K. Edwards, R. J. Shaver, L. Morgan, *Inorg. Chem.* **1990**, *29*, 167.
[16] M. A. Carvajal, S. Alvarez, J. J. Novoa, *Chem. Eur. J.* **2004**, *10*, 2117.
[17] R. Usón, J. Gimeno, L. A. Oro, J. M. Martinez del Ilardya, J. A. Cabeza, *J. Chem. Soc., Dalton Trans.* **1983**, 1729 and references cited therein.
[18] W. Kaiser, R. B. Saillant, W. N. Butler, P. G. Rasmusen, *Inorg. Chem.* **1976**, *15*, 2688.
[19] D. Walther, T. Döhler, N. Theyssen, H. Görls, *Eur. J. Inorg. Chem.* **2001**, 2049.
[20] L. Böttcher, D. Walther, H. Görls, *Z. Anorg. Allg. Chem.* **2003**, *629*, 1208.
[21] K. Lamm, M. Stollenz, M. Meyer, H. Görls, D. Walther, *J. Organomet. Chem.* **2003**, *681*, 24.
[22] S. Rau, K. Lamm, H. Görls, J. Schöffel, D. Walther, *J. Organomet. Chem.* **2004**, *689*, 3582.
[23] B. Dietzek, W. Kiefer, J. Blumhoff, L. Böttcher, S. Rau, D. Walther, U. Uhlemann, M. Schmitt, J. Popp, *Chem. Eur. J.* (manuscript submitted).
[24] COLLECT, Data Collection Software; Nonius B. V., Netherlands, **1998**.
[25] Z. Otwinowski, W. Minor, "*Processing of X-ray Diffraction Data Collected in Oscillation Mode*", in *Methods in Enzymology*, vol. 276, Macromolecular Crystallography, Part A (Eds.: C. W. Carter, R. M. Sweet), pp. 307–326, Academic Press, **1997**.
[26] SORTAV, R. H. Blessing, *Acta Crystallogr., Sect. A* **1995**, *51*, 33.
[27] G. M. Sheldrick, *Acta Crystallogr., Sect. A* **1990**, *46*, 467.
[28] G. M. Sheldrick, *SHELXL-97* (release 97-2), University of Göttingen, Germany, **1997**.
[29] CCDC-279790 (for **1**), -279791 (for **2**) and -286988 (for **3**) contain the supplementary crystallographic data for this paper. These data can be obtained free of charge from The Cambridge Crystallographic Data Centre via www.ccdc.cam.ac.uk/data_request/cif.
[30] See: M. Rudolph, *J. Comput. Chem.* **2005**, *26*, 1193 and references cited therein.

Received: December 21, 2005
Published Online: April 11, 2006

